



HAL
open science

Break-up dynamics of fluctuating liquid threads

Julien Petit, David Rivière, Hamid Kellay, Jean-Pierre Delville

► **To cite this version:**

Julien Petit, David Rivière, Hamid Kellay, Jean-Pierre Delville. Break-up dynamics of fluctuating liquid threads. Proceedings of the National Academy of Sciences of the United States of America, 2012, 109 (45), pp.18327-18331. 10.1073/pnas.1207634109 . hal-00751483

HAL Id: hal-00751483

<https://hal.science/hal-00751483>

Submitted on 13 Nov 2012

HAL is a multi-disciplinary open access archive for the deposit and dissemination of scientific research documents, whether they are published or not. The documents may come from teaching and research institutions in France or abroad, or from public or private research centers.

L'archive ouverte pluridisciplinaire **HAL**, est destinée au dépôt et à la diffusion de documents scientifiques de niveau recherche, publiés ou non, émanant des établissements d'enseignement et de recherche français ou étrangers, des laboratoires publics ou privés.

Break-up dynamics of fluctuating liquid threads

Julien Petit, David Rivière, Hamid Kellay, and Jean-Pierre Delville

Univ. Bordeaux, LOMA, UMR 5798, F-33400 Talence, France.

CNRS, LOMA, UMR 5798, F-33400 Talence, France.

Corresponding author: Jean-Pierre Delville

Address for correspondence:

Laboratoire Ondes et Matières d'Aquitaine

Université Bordeaux 1

351 Cours de la Libération

F-33400 Talence, France.

Email: jp.delville@loma.u-bordeaux1.fr

Phone: +33 5 40 00 62 10

Fax: +33 5 40 00 69 70

Classification: PHYSICAL SCIENCES, Physics

Abstract:

The thinning dynamics of a liquid neck before break-up, as may happen when a drop detaches from a faucet or a capillary, follows different rules and dynamic scaling laws depending on the importance of inertia, viscous stresses, or capillary forces. If now the thinning neck reaches dimensions comparable to the thermally excited interfacial fluctuations, as for nano-jet break-up or the fragmentation of thermally annealed nanowires, these fluctuations should play a dominant role according to recent theory and observations. Using near-critical interfaces, we here fully characterize the universal dynamics of this thermal fluctuation-dominated regime and demonstrate that the crossover from the classical two-fluid pinch-off scenario of a liquid thread to the fluctuation-dominated regime occurs at a well defined neck radius proportional to the thermal length scale. Investigating satellite drop formation, we also show that at the level of the crossover between these two regimes it is more probable to produce monodisperse droplets since fluctuation-dominated pinch-off may allow the unique situation where satellite drop formation can be inhibited. Nonetheless the interplay between the evolution of the neck profiles from the classical to the fluctuation-dominated regime and the satellites production remains to be clarified.

\body

Introduction

For a drop to detach from a capillary or a faucet, the liquid thread connecting them must thin and break. This break-up, or pinch-off, is an example of a singularity with well-established scaling laws and similarity solutions (1, 2, 3, 4, 5). Different regimes and scaling laws have been predicted and observed. For small liquid viscosities, the balance between inertia and capillarity leads to the so called inertial thinning regime with the thread radius vanishing as time to pinch-off to the power $2/3$. When the radius of the thinning thread becomes smaller than the so-called viscous length scale $L_\eta \sim \eta_{in}^2 / \gamma \rho_{in}$ (where γ , η_{in} and ρ_{in} are respectively the surface tension, the shear viscosity and the density of the fluid), viscous forces become important and the neck radius decreases linearly versus time (1) as $R(t) = CV_\eta(t^* - t)$, where $V_\eta \sim \gamma / \eta_{in}$ is a capillary velocity, C is a constant and t^* is the break-up time at neck pinch-off; a viscous time scale can be defined as $\tau_\eta \sim L_\eta / V_\eta$. Two thinning regimes have been predicted and observed in this case: the so-called visco-capillary regime at low Reynolds numbers exhibiting symmetric necks with $C = 0.071$ (6) and the visco-capillary-inertial regime emerging when further thinning significantly increases the inner fluid velocity and thus inertia (7). In this latter case, the constant is $C = 0.030$ and the neck profiles are asymmetric. Note that more recently, other symmetric break-up dynamics have been found for a class of non Newtonian fluids for which thinning is dictated by the rheological properties of the fluids (8, 9).

When the viscosity of the outer fluid is no more negligible, as in the present investigation, the thinning dynamics is dominated by visco-capillary stresses when the radius of the rupturing neck $R(t) < \frac{\eta_{out}}{\eta_{in}} L_\eta$ (1), where η_{out} is the shear viscosity of the fluid outside the thread. The variation of the radius again

obeys a linear scaling law $R(t) = HV_\eta(t^* - t)$, where $H(\eta_{in}/\eta_{out})$ is a function which was experimentally (2) and theoretically evaluated (10, 11). In this two fluid visco-capillary regime, the thinning neck is asymmetrical, eventually leading to the formation of satellite droplets.

While these different regimes consider the interface as smooth even at the smallest scales examined, recent simulations of nanojet break-up (12, 13) as well as theoretical (14) and experimental work (15) revealed that the interface roughness due to the interfacial thermal fluctuations may play a dominant role in liquid column break-up when $R(t) < L_T$, where $L_T = \sqrt{k_B T / \gamma}$ is the so-called thermal length scale estimated by comparing the thermal energy $k_B T$ to the surface tension γ . In this case, the thinning neck is predicted to be symmetrical with respect to the break-up location, thus minimizing the formation of satellite drops at pinch-off (13, 14). Moreover, the thinning of the neck is predicted to follow the scaling law $R(t) \propto (t^* - t)^{0.42}$ (14), where the proportionality factor remains to be determined theoretically and experimentally (14, 15). Since the thermal length is classically in the range of a few molecules, observation of this thinning regime in a laboratory scale experiment requires a significant increase of L_T . A route for fulfilling this condition is the use of near-critical binary fluids with strongly fluctuating interfaces (16) which offer the unique opportunity of reaching strongly fluctuating hydrodynamic regimes.

Results

The experiment is performed in a near-critical phase-separated water-in-oil micellar phase of a microemulsion whose mass composition is adjusted to be critical at a temperature $T_C = 308 \text{ K}$. The fluid preparation and properties are detailed in the Supporting Information text. For a temperature $T > T_C$, the mixture separates in two coexisting phases of different micellar concentrations separated by an interface

which has large thermally-induced interfacial fluctuations near T_C . Two main reasons motivated this choice of system. (i) Due to the supramolecular nature of the micelles, the bulk correlation length of

density fluctuations $\xi^- = \xi_0^- \left(\frac{T - T_C}{T_C} \right)^{-0.63}$ is intrinsically large, allowing interfacial fluctuations to be

observable optically. (ii) It follows from the universal ratio $\mathfrak{R}^- = \frac{\gamma(\xi^-)^2}{k_B T_C} = 0.108$ (17), that the interfacial

tension $\gamma = \gamma_0 \left(\frac{T - T_C}{T_C} \right)^{1.26}$ is extremely weak compared to that of usual liquid mixtures. For

$(T - T_C) = 0.1 K$, one finds $L_\eta \sim 46 cm$ and $\tau_\eta \sim 1.5 \cdot 10^5 s$ on the one hand, and $L_T \approx 1 \mu m$ as

$L_T = \xi^- / \sqrt{\mathfrak{R}^-} = 3\xi^-$ on the other hand. Moreover, considering ξ^- as the relevant length scale, the

corresponding relaxation time scale $\tau_\xi \approx \frac{6\pi\eta_{out}(\xi^-)^3}{k_B T} \approx 0.2 s$ is orders of magnitude larger than in usual

molecular liquids. Neck thinning driven by thermal fluctuations thus becomes experimentally accessible.

The second key point of the experiment requires starting with an initially stable and well-controlled liquid column to properly fix initial conditions and boundary effects before further destabilization. While large aspect ratio liquid columns are known to be unstable due to the Rayleigh-Plateau instability (3), it is briefly shown in the Supporting Information text that this fundamental limitation can be circumvented using the radiation pressure of a continuous laser beam to deform the meniscus separating the coexisting phases (18), which is located in the middle of the sample due to near-criticality. For a sufficient beam power, the surface deformation ends up connected to the bottom glass face of the cell, thus forming a large aspect ratio liquid column whose diameter is controlled by the incident beam power. Hydrodynamic stabilization is provided through the radiation pressure exerted by the beam propagation inside the column (19). Fig. 1A illustrates the regularity of such a laser-sustained liquid column.

Once formed, the column is left to relax after turning off the laser beam, as illustrated in Figs. 1B-C. To avoid boundary effects, we focus on a mid-column rupture event, as that indicated by the horizontal arrow in Fig. 1C. We record the neck thinning dynamics with a $50\times$ Olympus microscope objective ($NA = 0.45$) coupled to a video camera (2560×1600 pixels) operating at variable frame rates. Figs. 1D-F illustrate a typical thinning morphology with particular emphasis on the observed neck symmetry and the inhibition of satellite drop formation in this case. Note however, the occurrence of a more elongated neck below the one selected for a close-up; such a neck may lead to satellite drop formation as it may break at more than one location. Fig. 2 presents the thinning dynamics of a column for $(T - T_C) = 0.23 K$. The determination of the neck radius is detailed in the Materials and Methods section. After the first stages of the Rayleigh-Plateau instability, the neck radius $R(t^* - t)$ starts to decrease linearly in time as expected for two-fluid visco-capillary thinning (see Inset of Fig. 2). Beyond a crossover at $(t^* - t) \approx 0.34 s$ and $R(t^* - t) \approx 0.8 \mu m$, i.e. $(t^* - t)/\tau_{\xi^-} \approx 8$ and $R(t^* - t)/\xi^- \approx 4$, the thinning dynamics switches to a power law behavior, well approximated by $R \sim (t^* - t)^{0.42}$, up to break-up; a power law fit gives 0.43 .

To confirm the robustness of the observed thinning dynamics, we first investigate the two-fluid visco-capillary behavior. The variation of $R(t^* - t)$ measured for each $(T - T_C)$ is fit linearly to extract the break-up time t_η^* expected for pure two-fluid visco-capillary thinning. Data are then reanalyzed in terms of reduced length and time scales, respectively R/L_η and $(t_\eta^* - t)/\tau_\eta$, to focus on this regime. Note that we should have used the length scale $\frac{\eta_{out}}{\eta_{in}} L_\eta$ but close to the critical point $\eta_{in} \sim \eta_{out} \sim \eta_C$, the viscosity at criticality. As shown in Fig. 3, the measurements all fall onto a single master straight line over more than

one order of magnitude in rescaled length and time scales. We extract $H(\eta_{in}/\eta_{out} = 1) \approx (2.9 \pm 1) 10^{-2}$ from the fit of the whole data set exhibiting a linear regime, illustrated in the Inset of Fig. 3, which is in agreement with previous measurements $H(\eta_{in}/\eta_{out} = 1) \approx (3.3 \pm 1) 10^{-2}$ (2). Note that this rescaling requires confidence in the value of the interfacial tension $\gamma(T - T_C)$ which is here deduced from \mathfrak{R}^- and the set value of $(T - T_C)$. However, weak temperature variations around the set point as well as minor deviations from the set composition of the sample can produce large relative variations of γ for temperatures close to T_C . Consequently, some experiments were preceded by in situ contactless measurements of the interfacial tension from the meniscus deformation by the optical radiation pressure at a very low beam power. As briefly discussed in the Supporting Information text, this method leads to a relative uncertainty $\leq 20\%$ for γ which de facto has an incidence on the determination of $H(\eta_{in}/\eta_{out} = 1)$ from the linear slope $\gamma H(1)/\eta_{in}$ expected for the visco-capillary regime.

Eventually, the neck thinning deviates from the linear visco-capillary behavior and accelerates during the last instants indicating the presence of an additional more efficient mechanism operating at small length scales and expected when interfacial fluctuations play a role. Although small scales may be difficult to determine (See the Materials and Methods section), the fact that this deviation appears systematically for a wide range of conditions signals the onset of a different rupture regime. To further investigate this regime, the data set for all $(T - T_C)$ examined is now rescaled with the correlation length and time scales, R/ξ^- and $(t^* - t)/\tau_{\xi^-}$. Fig. 4 shows that data rescaling leads to a single behavior up to the crossover with the visco-capillary dynamics. The fit of the whole data set belonging to this regime is illustrated in the left

Inset of Fig. 4 and gives $R = A_{\xi^-} \xi^- \left(\frac{t^* - t}{\tau_{\xi^-}} \right)^{0.42}$ with $A_{\xi^-} = 1.61$, when forcing the exponent to its predicted

value 0.42 . A free-parameter nonlinear fit leads to $A_{\xi^-} = 1.71$ and an exponent 0.37 . The existence of a universal thermal fluctuation-dominated regime is thus firmly demonstrated by finding, over two orders of magnitude in rescaled time, a robust exponent close to the numerically calculated one 0.42 . Our data also allow a measurement of the amplitude A_{ξ^-} over a wide range of conditions and show that the relevant length and time scales for this pinching regime are indeed the correlation length and its relaxation time.

Fig. 4 also shows that the crossover from the visco-capillary to the thermal fluctuation dominated regime appears as an inflexion point at a well-defined range in rescaled time and radius, centered around $(t^* - t)_{crossover} / \tau_{\xi^-} \approx 6$ and $R_{crossover} / \xi^- \approx 3$, i.e. $R_{crossover} \approx L_T$. The crossover to the fluctuation-dominated regime therefore occurs at scales comparable to the height fluctuations of the interface, which in this case are simply proportional to the bulk correlation length ξ^- . Again and despite the difficulty of extracting such small values of the neck radii, a systematic variation in ξ^- of the crossover radius is observed. One may argue that this crossover originates from a balance between the driving capillary pressure and the additional pressure in the neck due to the fluctuating interface. Neglecting the axial curvature, the Laplace pressure inside the neck is γ/R . Besides, the thermal energy density in an elementary cylinder of radius R and length $\xi_{||}^-$ is given by $\frac{k_B T}{\pi R^2 \xi_{||}^-}$, where $\xi_{||}^-$ represents the axial correlation length of the interface fluctuations which is proportional to ξ^- (20). Since $k_B T_c / \gamma = (\xi^-)^2 / \mathfrak{R}^-$ (17), this balance occurs for R proportional to ξ^- . We identify this radius as the crossover between the two regimes. The right Inset of Fig. 4 shows that $R_{crossover}(\xi^-)$ is indeed consistent with a linear variation $R_{crossover} = 3.5 \xi^-$.

Discussion

Besides being of importance as it tackles the difficult problem of hydrodynamics of strongly fluctuating media (21), the thermal fluctuation dominated pinch-off regime is supposed to have clear repercussions on the formation of satellite drops. To shed light on this issue, we considered different $(T - T_C)$, to tune the amplitude of fluctuations, and different beam powers and waists to modify the mean radius R_0 of the initial light-sustained liquid column. This column ends up breaking into a number of main drops due to the Rayleigh-Plateau instability (4) when light is turned off. Besides these main drops, smaller droplets may appear in between which are referred as to as satellite drops. The images of Fig. 5A-C show that the number of satellites depends on the ratio between the initial radius R_0/ξ^- : the smaller this ratio the smaller the number of satellites. The latter are basically absent in Fig. 5A where only the main drops are present while farther away in temperature from the critical point, they are systematically present. In order to quantify this observation, we present in Fig. 5D, the fraction of satellite drops, defined as the ratio of the number of satellite drops to the number of necks between main drops, versus R_0 . This figure shows that the mean satellite fraction is roughly unity for $R_0/\xi^- \sim 50$ (an example of an almost bi-disperse situation can be seen in Fig. 5B), and strongly fluctuates in the range $R_0/\xi^- \sim 60 - 80$ from one experiment to another, and along the same liquid thread as illustrated in Fig. 5C where zero, one and two-satellite events are present in the same snapshot.

Most important is that this satellite fraction is a decreasing function of R_0 and goes to zero when R_0 becomes smaller than a cutoff value $R_{\xi^-} \approx 10\xi^-$ (a linear fit leads to $R_{\xi^-}/\xi^- = 13$). This decrease and the fact that R_{ξ^-} is close to $R_{crossover}$, both point to the major role of thermal fluctuations in preventing satellite drop formation. Nonetheless, the exact details of the evolution of the neck profile from asymmetric in the two-fluid visco-capillary regime to symmetric in the fluctuation-dominated regime and its link to the decrease of the satellite fraction in Fig. 5D remains to be elucidated. In addition, as noted in Fig. 1C,

elongated necks may coexist with symmetric ones in the fluctuation dominated regime leading to the presence of a small number of satellite drops (as for $(T - T_C) = 0.1 K$ in Fig. 5D). While the fluctuation-dominated regime does inhibit satellite drop formation, the subtle interplay between the temporal evolution of the neck shape and the production of these satellites in presence of fluctuations calls for additional theoretical and experimental work.

In conclusion, we have demonstrated the robustness of the signature of thermal fluctuations on the thinning dynamics of liquid necks, as well as the existence of a well-defined crossover to this regime. Our measurements bring a quantitative description of this regime in a near critical fluid. Since the existence of this regime requires self similar solutions, our results bring support to their relevance even in strongly fluctuating systems. We have also shown that the consequences of such fluctuation-dominated thinning can be quite important for the production of satellite drops as predicted (12, 14) even though how this works precisely remains to be addressed. This property may be useful to produce monodisperse drops at very small scales with examples ranging from nanojet devices such as carbon nanotube channels (22) to the fragmentation of nanowires by thermal annealing (23) for creating chains (24) or patterns (25) of monodisperse nanoparticles.

Materials and Methods

Measuring the minimum neck radius

This measurement is carried out using movies of the break-up of the chosen liquid neck taken at frame rates between 100 and 500 frames per second. An example is given in Fig. 6 for $(T - T_C) = 0.3 K$. First, and as depicted by the rectangular window in Fig. 6A, the images are inspected to visually delimit the region of minimal neck diameter. The intensity profile in the direction perpendicular to the neck is then

measured and averaged over the few pixels of the depicted window along the direction of the neck. This intensity profile is fit to a Gaussian up to the black stripes associated with the interface. By translating the window along the neck over which the intensity profile is measured and averaged, different Gaussian widths can be measured and we select the minimum width at half maximum as the minimum neck diameter. The resulting intensity profile corresponding to Fig. 6A is reported versus distance in pixels in Fig. 6F row (a). At the used magnification, each pixel corresponds to $0.1 \mu\text{m}$. Intensity profiles are then measured at successive times. Several images as well as their associated profiles are shown in Fig. 6 at different times before rupture; rows (a), (b), (c), (d) and (e) in Fig. 6F correspond to snapshots (A), (B), (C), (D) and (E). As the diameter becomes smaller and smaller, this determination becomes more and more difficult since the profiles become less well defined. Still such a procedure remains quite reasonable down to at least $0.6 \mu\text{m}$ in diameter as shown in Fig. 6E. Diameters below $0.4 \mu\text{m}$ become very difficult to measure as the contrast between the neck and the outer medium becomes very small. Further inspection of the rupture region, nevertheless, allows estimating the final rupture time.

References

1. Lister J R, Stone H A (1998) Capillary breakup of a viscous thread surrounded by another viscous fluid. *Phys Fluids* 10: 2758-2754.
2. Cohen I, Nagel S R (2001) Testing for scaling behavior dependence on geometrical and fluid parameters in the two fluid drop snap-off problem. *Phys Fluids* 13: 3533-3541.
3. Eggers J (1997) Nonlinear dynamics and breakup of free-surface flows. *Rev Mod Phys* 69: 865-929.
4. Eggers J, Villermaux E (2008) Physics of liquid jets. *Rep Prog Phys* 71: 036601.1-49.
5. Basaran O A (2002) Small-scale free surface flows with breakup: drop formation and emerging applications. *AIChE Journal* 48: 1842-1848.
6. Papageorgiou D T (1995) On the breakup of viscous liquid threads. *Phys. Fluids* 7: 1529-1544.

7. Eggers J (1993) Universal Pinching of SD Axisymmetric Free-Surface Flow. *Phys. Rev. Lett.* 71: 3458-3460.
8. Suryo R, Basaran O A (2006) Local dynamics during pinch-off of liquid threads of power law fluids: Scaling analysis and self-similarity. *J. Non-Newtonian Fluid Mech.* 138: 134–160.
9. Savage J R, Caggioni M, Spicer P T, Cohen I (2010) Partial universality: pinch-off dynamics in fluids with smectic liquid crystalline order. *Soft Matter* 6: 892–895.
10. Cohen I, Brenner M P, Eggers J, Nagel S R (1999) Two Fluid Drop Snap-Off Problem: Experiments and Theory. *Phys Rev Lett* 83: 1147-1150.
11. Zhang W W, Lister J R (1999) Similarity Solutions for Capillary Pinch-Off in Fluids of Differing Viscosity. *Phys Rev Lett* 83: 1151-1154.
12. Moseler M, Landman U (2000) Formation, stability, and breakup of nanojets. *Science* 289: 1165-1169.
13. Landman U (2005) Materials by numbers: Computations as tools of discovery, *Proc Natl Acad Sci USA* 102: 6671–6678.
14. Eggers J (2002) Dynamics of liquid nanojets. *Phys Rev Lett* 89: 084502.1-4.
15. Hennequin Y, Aarts D G A L, Van der Wiel J H, Wegdam G, Eggers J, Lekkerkerker H N W, Bonn D (2006) Drop formation by thermal fluctuations at an ultralow surface tension. *Phys Rev Lett* 97: 244502.1-4.
16. Aarts D G A L, Schmidt M, Lekkerkerker H N W (2004) Direct Visual Observation of Thermal Capillary Waves. *Science* 304: 847-850.
17. Moldover M R (1985) Interfacial tension of fluids near critical points and two-scale-factor universality. *Phys Rev A* 31: 1022-1033.
18. Wunenburger R, Casner A, Delville J P (2006) Light-induced deformation and instability of a liquid interface. I. Statics. *Phys Rev E* 73: 036314.1-16.

19. Brasselet E, Wunenburger R, Delville J P (2008) Liquid Optical Fibers with a Multistable Core Actuated by Light Radiation Pressure. *Phys Rev Lett* 101: 014501.1-4.
20. Indekeu J O, Aarts D G A L, Lekkerkerker H N W, Hennequin Y, Bonn D (2010) Thermal fluctuation forces and wetting layers in colloid-polymer mixtures: Derivation of an interface potential. *Phys Rev E* 81: 041604.1-12.
21. Assenheimer M, Steinberg V (1994) Transition between spiral and target states in Rayleigh–Bénard convection. *Nature* 367: 345-347.
22. Mattia D, Gogotsi Y (2008) Review: static and dynamic behavior of liquids inside carbon nanotubes. *Microfluid Nanofluid* 5: 289-305.
23. Toimil Molarasa M E, Balogh A G, Cornelius T W, Neumann R, Trautmann C (2004) Fragmentation of nanowires driven by Rayleigh instability. *Appl Phys Lett* 85: 5337-5339.
24. Chen J T, Zhang M, Russell T P (2007) Instabilities in nanoporous media. *Nano Lett* 7: 183-187.
25. Park H, Russell T P, Park S (2010) Spatial control of dewetting: highly ordered teflon nanospheres. *J Colloid Interface Sci* 348: 416-423.

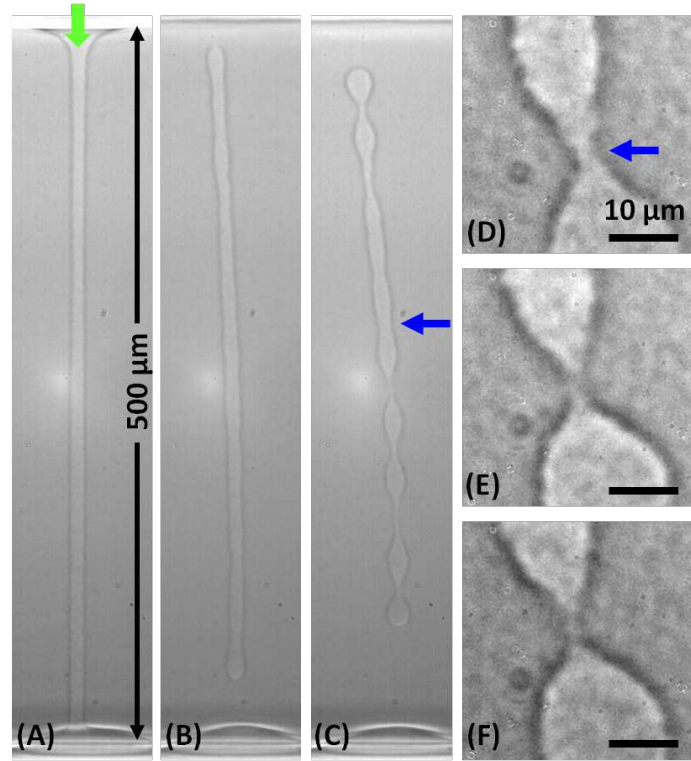


Figure 1: (A) Initial large aspect ratio column ($L/R_0 = 50$) formed in a 1 mm thick cell at $(T - T_C) = 0.28\text{ K}$ and stabilized optically between the near-critical meniscus on top and the bottom face of the cell. The vertical arrow indicates incidence of the frequency-doubled $Nd^{3+} - YAG$ continuous wave laser beam (wavelength in vacuum $\lambda_0 = 532\text{ nm}$) of waist $\omega_0 = 2.5\text{ }\mu\text{m}$ and power $P = 200\text{ mW}$ used to produce the column. The picture is captured just before laser interruption. (B) Column destabilization 4 s after laser interruption; note the fast pinch-off at the boundaries. (C) Column 8 s after laser interruption; the horizontal arrow indicates the neck under study taken near the middle of the liquid column. (D-F) Close-up view of the neck thinning 2 s , 0.2 s and 0.02 s before break-up. Note the roughness of the interface, which is a direct signature of the thermal fluctuations close to a critical point.

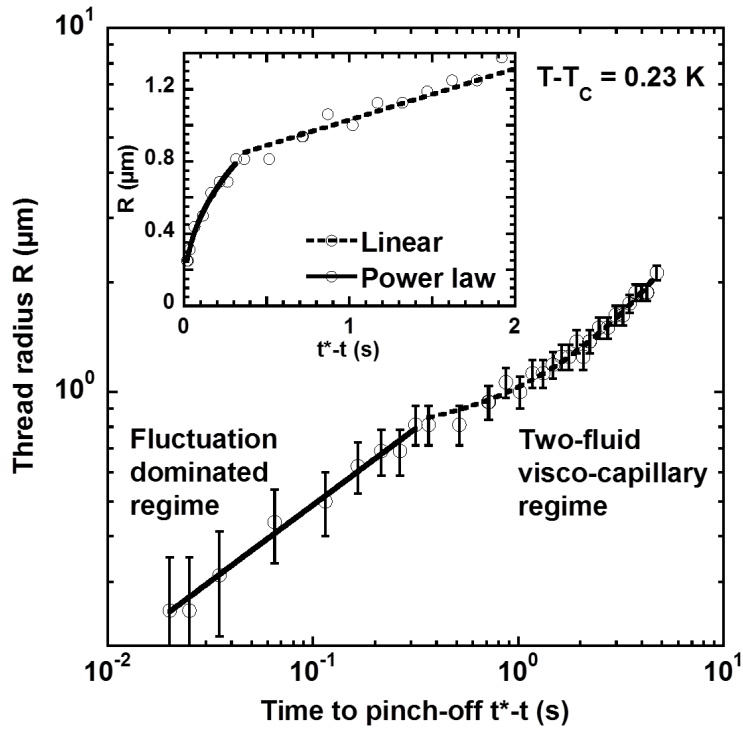


Figure 2: Log-Log plot of the time variation of the neck thinning up to break-up at $(T - T_c) = 0.23 \text{ K}$. A linear plot is presented in the Inset with duration of the linear regime which has been deliberately reduced to highlight the transition toward a power law behavior. The visco-capillary and the fluctuation-dominated regimes are respectively fit to a linear function and a power law with exponent forced at 0.42 . The error bars correspond to a measurement error of $0.2 \mu\text{m}$ on the diameter.

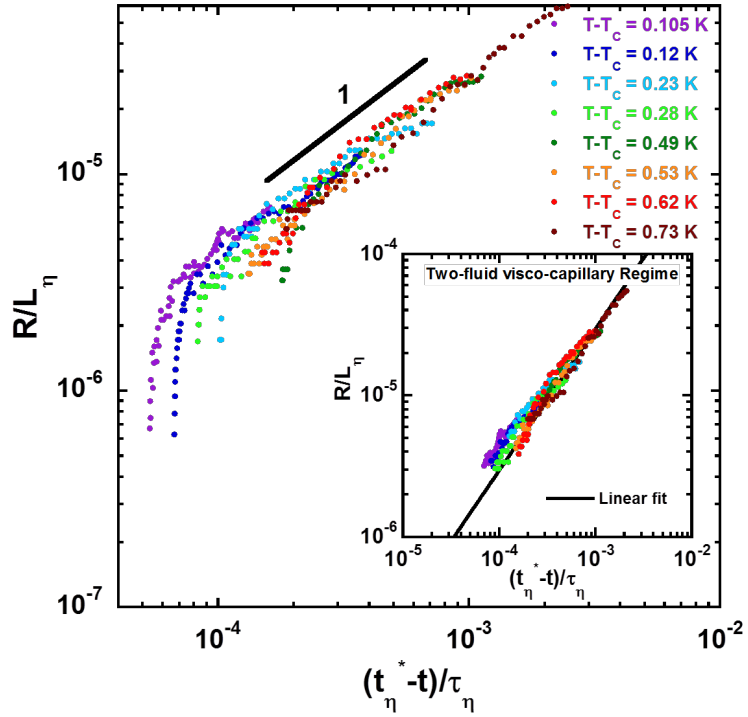


Figure 3: Universal thinning dynamics in the visco-capillary regime. The measured breakup time t^* is replaced by the breakup time t_η^* that would be expected for pure visco-capillary break up, and the dynamics is presented in radius and time reduced with the viscous length L_η and characteristic time τ_η over a seven-fold variation in $(T - T_c)$. Inset: fit of the whole set of data belonging to the visco-capillary regime.

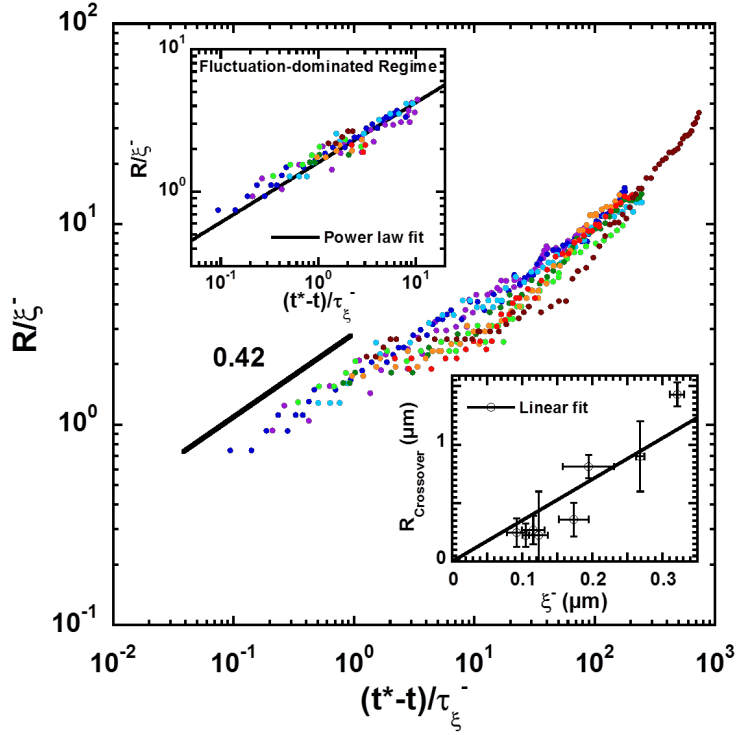


Figure 4: Universal thinning dynamics in the thermal fluctuation-dominated regime (same color convention as in Fig. 3). The dynamics is presented in radius and time reduced with the correlation length ξ^- and relaxation time τ_{ξ^-} . Left Inset: power law fit, with exponent forced to 0.42 , of the whole set of data belonging to the thermal fluctuation regime. Right Inset: Variation of the neck radius at the thinning regime crossover $R_{crossover}$ versus ξ^- ; the error bars add the statistical determination by different methods (best fits around the crossover and largest temporal window) and the measurement error.

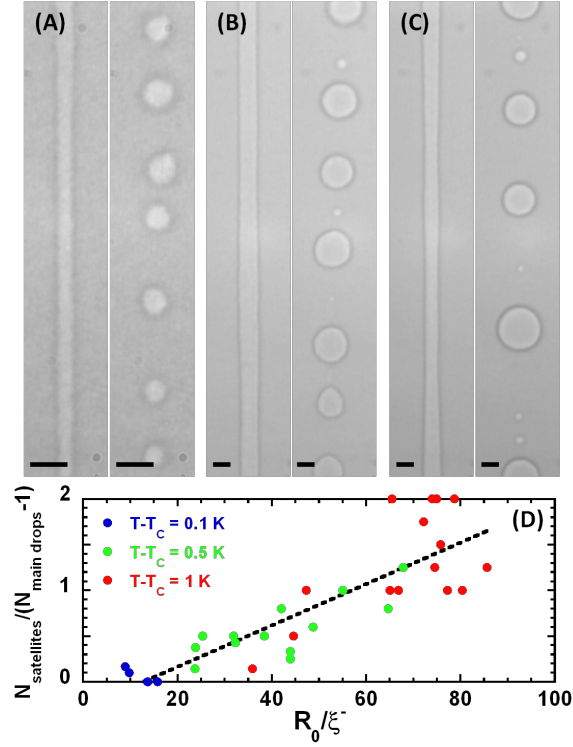


Figure 5: (A-C) Typical liquid thread before and after destabilization for different $(T - T_C)$. (A) $(T - T_C) = 0.1 K$, and a laser beam of waist $\omega_0 = 1.4 \mu m$ and power $P = 130 mW$ to produce a liquid column of rescaled radius $R_0 / \xi^- = 15.8$; note the absence of satellite drops. (B) $(T - T_C) = 0.5 K$, $\omega_0 = 3.0 \mu m$ and $P = 200 mW$ leading to $R_0 / \xi^- = 55.1$; note the production of an almost bi-disperse drop distribution. (C) $(T - T_C) = 1 K$, $\omega_0 = 3.0 \mu m$ and $P = 200 mW$ leading to $R_0 / \xi^- = 65.0$; note the simultaneous presence of zero, one and two-satellite events keeping a satellite fraction close to one. The interface roughness increase due to the interfacial thermal fluctuations can also be noticed from (C) to (A) when the critical point is neared. The scale bars in (A-C) represent $20 \mu m$. (D) Variation of the satellite fraction versus rescaled radius of the initially optically stabilized liquid column R_0 / ξ^- ; the dashed linear fit is a guide to the eye.

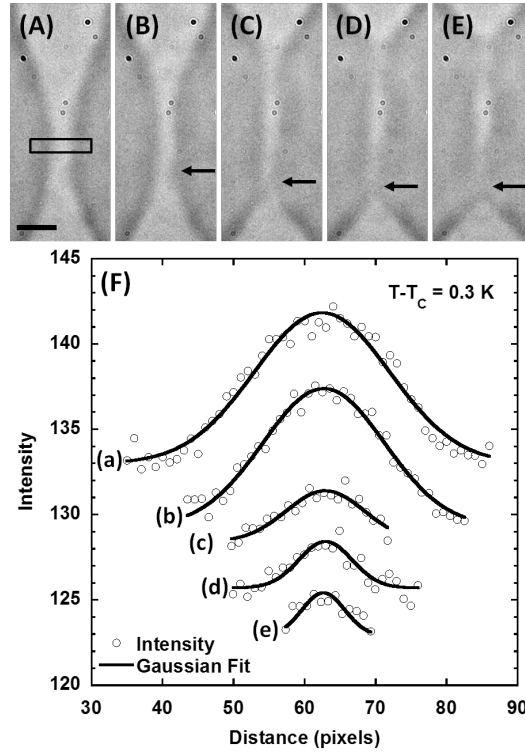


Figure 6: The photographs from (A) to (E), extracted from an experiment performed at $(T - T_c) = 0.3 K$, show a close up of the neck region to be analyzed to measure the minimum neck diameter and therefore the minimum neck radius used in this study; the scale bar in (A) represents $5 \mu m$. The images correspond to (A) 0.86s, (B) 0.56s, (C) 0.17s, (D) 0.08s, and (E) 0.02s before estimated rupture time. The associated intensity profiles are obtained by averaging along the direction perpendicular to the symmetry axis of the neck over the few pixels of the window indicated in (A). These profiles are fit to a Gaussian whose minimum width is obtained by moving the window up and down. (F) illustrates these fits, respectively denoted (a-e) in correspondence to (A-E) and arbitrarily shifted in intensity; the corresponding widths are: (a) $19 px$, (b) $17 px$, (c) $11 px$, (d) $7.5 px$ and (e) $6 px$. The minimum diameter, from which the minimum neck radius is obtained to plot the thinning dynamics of the neck versus time, is taken to be the width at half maximum of the Gaussian fit, i.e. the minimum width of the Gaussian is multiplied by $\sqrt{\ln 4}$.

Supporting Information

Petit et al. Break-up dynamics of fluctuating liquid threads

Near-Critical Micellar Phases of Microemulsion

We used a near-critical phase-separated micellar solution of a microemulsion because, as illustrated below, supra-molecular liquids have many advantages when investigating hydrodynamics near a critical point. The chosen microemulsion is a four components liquid mixture composed of water, oil (toluene), surfactant (sodium-dodecylsulfate, SDS), and cosurfactant (n-butanol-1). At low concentrations in water and surfactant, the quaternary mixture can in fact be considered as binary since it organizes at thermodynamic equilibrium as a suspension of surfactant-coated water nanodroplets, the micelles, dispersed in a continuum mainly composed of toluene. In the considered part of the phase diagram, a line of low critical points exists, the coexistence curves being inverted as compared to the usual case (1). For the chosen composition (toluene: 70% wt, water: 9% wt, SDS: 4% wt, and butanol: 17% wt), the micelle size, given by the amplitude factor of the correlation length of density fluctuations, is $\xi_0^+ = 40 \text{ \AA}$ (2). This value is sufficiently small for the mixture to be transparent in the visible range and large enough, typically ten times that of classical fluids, to facilitate observation of critical opalescence. This micellar phase of microemulsion is isotropic and belongs to the universality class ($d = 3, n = 1$) of the Ising model (3), as most of classical liquid mixtures. For the chosen composition, the critical temperature is $T_C \approx 35 \text{ }^\circ\text{C}$. Above T_C , the mixture separates in two micellar phases of different micelle concentrations $\Phi_{i=1,2}$, as indicated in the schematic phase diagram shown in Fig. S1 A. Many fluid properties present scaling-law behavior in $(T - T_C)$ near the critical point. Of interest for the present investigation are:

1) The bulk correlation length of density fluctuations in the two-phase region: $\xi^- = \xi_0^- \left(\frac{T - T_C}{T_C} \right)^{-\nu}$ with

$$\nu = 0.63 \text{ and } \xi_0^- = \xi_0^+ / 1.9 = (21 \pm 1) \text{ \AA}.$$

2) The coexistence curve, assumed to be symmetric close to the critical point:

$$\Phi_{i=1,2} = \Phi_C + (-1)^i \frac{\Delta\Phi_0}{2} \left(\frac{T - T_C}{T_C} \right)^\beta \text{ with } \beta = 0.325, \Phi_C = 0.11 \text{ and } \Delta\Phi_0 = 0.42.$$

3) The density of the coexisting phases: $\rho_{i=1,2} = \rho_{mic} + \rho_{cont} (1 - \Phi_i)$, where $\rho_{mic} = 1045 \text{ kg/m}^3$ and $\rho_{cont} = 850 \text{ kg/m}^3$ are respectively the densities of the micelles and the surrounding oil continuum.

4) The interfacial tension between the coexisting phases: $\gamma = \gamma_0 \left(\frac{T - T_C}{T_C} \right)^{2\nu}$ with

$$\gamma_0 = 0.108 \text{ } k_B T_C / \left(\frac{\xi_0^-}{\xi_0^+} \right)^2 \text{ } 10^{-4} \text{ N.m}^{-1} \text{ (4).}$$

5) The shear viscosity of the coexisting phases: $\eta_{i=1,2} = [1.460 - 0.014(T - 273.15)](1 + 2.5\Phi_i)10^{-3}$ (5)

6) The optical absorption at the used wavelength: $\alpha_{abs}(\lambda_0 = 532 \text{ nm}) \approx 0.03 \text{ m}^{-1}$, which prevents the mixture from laser heating at the used beam powers.

Generating Liquid Columns

The experimental procedure to produce stable liquid columns is presented in Fig. S1 B. A laser beam is focused on the meniscus of the phase-separated mixture (contained in a 1 or 2 mm thick sealed Hellma cell) using a 10× Olympus microscope objective ($NA = 0.25$). The beam power and the beam waist ω_0 can be changed using various optical components. As the interfacial tension of near-critical interfaces is extremely weak, meniscus deformations are induced by the radiation pressure of the continuous laser beam, here a frequency-doubled $Nd^{3+} - YAG$ (wavelength in vacuum $\lambda_0 = 532 \text{ nm}$) in the TEM_{00} mode. The interface bending direction does not depend on beam propagation because photons gain momentum

when crossing the interface from a low to a large refractive index medium. Consequently, momentum conservation always leads to a meniscus bending toward the fluid of smallest index of refraction, i.e. here from Φ_2 to Φ_1 , since (i) Φ_2 is the liquid phase of lowest micellar concentration and (ii) the index of refraction of toluene is larger than that of water. Nonetheless, the generation of stable liquid columns (Fig. S1 C-D) requires a beam incidence from the fluid of largest index of refraction (6), i.e. the liquid phase Φ_2 . The beam should then propagate downward as indicated by the arrow in Fig. S1 C. Above a beam power threshold, the bended meniscus becomes unstable, forms a jet and produces a stable liquid column when the jet tip reaches the bottom face of the cell containing the sample. Comparison between Fig. S1 C and Fig. S1 D shows that the column radius can be tuned by varying the beam power.

Observations are performed from the side using a focused white light source for illuminating the sample and a $50\times$ Olympus microscope objective ($NA = 0.45$) for imaging using a video camera and recording the destabilization of the liquid columns when the laser is turned off. A spectral filter is also placed between the microscope and the camera to eliminate the laser light scattered by the micellar phases near the critical point.

Contactless measurement of the interfacial tension

The measurement of ultra-low interfacial tensions is very difficult by usual contact techniques. We thus used the radiation pressure of the laser beam at low beam power to deform the meniscus separating the two coexisting phases and deduce γ at a given $(T - T_c)$ from the stationary deformation height $h(r = 0)$ on beam axis (7). In the weak deformation regime ($\partial h / \partial r \ll 1$), this height is given by:

$$h(r = 0) = \left(\frac{2P}{cg\pi\omega_0^2} \right) \left(\frac{\partial n}{\partial \rho} \right)_T \frac{\omega_0^2}{8l_c^2} \exp\left(\frac{\omega_0^2}{8l_c^2} \right) E_1\left(\frac{\omega_0^2}{8l_c^2} \right), \text{ where } (\partial n / \partial \rho)_T \text{ is the refractive index variation}$$

with density, $l_c = \sqrt{\frac{\gamma}{(\rho_1 - \rho_2)g}}$ is the capillary length and $E_1(x)$ is the Exponential Integral function (8).

For example, we find $h(r=0) = -5.5 \pm 0.3 \mu\text{m}$ for an experiment performed at $(T - T_C) = 0.3 \text{ K}$, $\omega_0 = 7.48 \mu\text{m}$ and $P = 33 \text{ mW}$, and $h(r=0) = -8.0 \pm 0.3 \mu\text{m}$ at $(T - T_C) = 0.4 \text{ K}$, $\omega_0 = 7.48 \mu\text{m}$ and $P = 66 \text{ mW}$; the uncertainties on $h(r=0)$ results from the use of a $20\times$ objective, instead of $50\times$, for imaging the entire interface deformation. We respectively deduce $\gamma \approx 1.8 \cdot 10^{-8} \text{ N/m}$ and $\gamma \approx 2.6 \cdot 10^{-8} \text{ N/m}$. Taking into account the uncertainty on $h(r=0)$, the estimation of $(\partial n / \partial \rho)_T$ from the Clausius-Mossotti relation, and the relative error $\leq 10\%$ on $(T - T_C)$ at $(T - T_C) = 0.3 - 0.4 \text{ K}$, we find a deviation $\leq 20\%$ on γ compared to the value calculated from the universal ratio \mathfrak{R}^- .

References

1. Meunier J, Cazabat A M, Langevin D, Pouchelon A (1982) Critical behaviour in microemulsions, *J. Phys. (France) Lett.* 43: L89-L95.
2. Freysz E, Laffon E, Delville J P, Ducasse A (1994) Phase conjugation in critical microemulsions. *Phys Rev E* 49: 2141-2149.
3. Jean-Jean B, Freysz E, Ducasse A, Pouligny B (1988), Thermodiffusive and electrostrictive optical nonlinearities in critical microemulsions, *Europhys.Lett.* 7: 219-224 (1988).
4. Moldover M R (1985) Interfacial tension of fluids near critical points and two-scale-factor universality. *Phys Rev A* 31: 1022-1033.
5. Wunenburger R, Issenmann B, Brasselet E, Loussert C, Hourtane V, Delville J P (2011), Fluid flows driven by light scattering, *J. Fluid Mechanics* 666: 273-307.
6. Wunenburger R, Casner A, Delville J P (2006) Light-induced deformation and instability of a liquid interface. I. Statics. *Phys Rev E* 73: 036314.1-16.
7. Mitani S, Sakai K (2002) Measurement of ultralow interfacial tension with a laser interface manipulation technique. *Phys. Rev. E* 66: 031604.1-6.

8. Wunenburger R, Casner A, Delville J P (2006) Light-induced deformation and instability of a liquid interface. I. Statics. *Phys Rev E* 73: 036314.1-16.

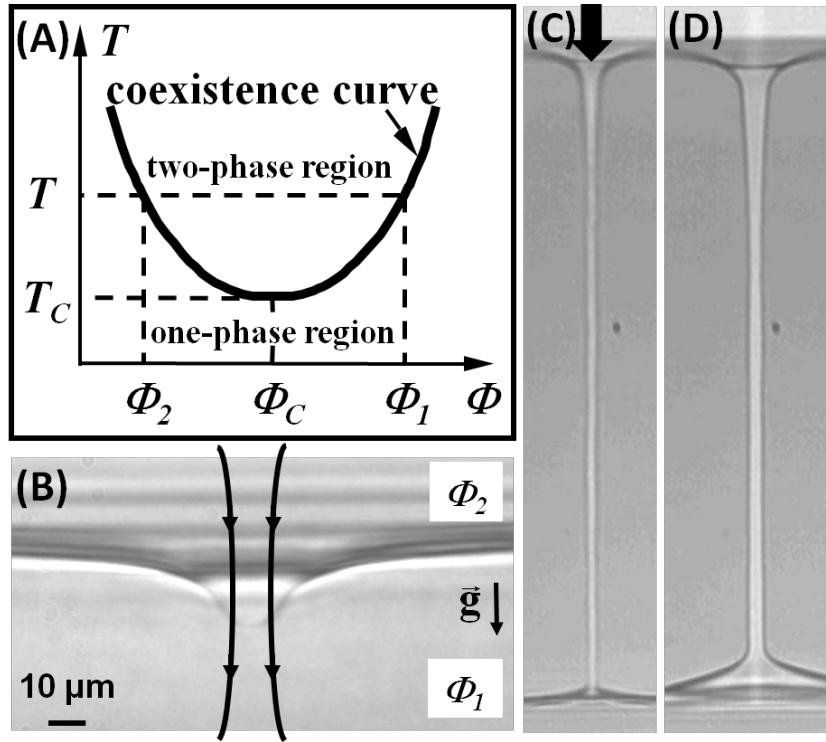


Figure S1: (A) schematic phase diagram of the micellar phase of microemulsion used. T is temperature and Φ is the volume fraction of micelles; T_C is the critical temperature and Φ_1 and Φ_2 are respectively the volume fractions of the micelle rich and the poor phases in coexistence. (B) Experimental configuration for a temperature $T > T_C$. The optical bending of the meniscus of the phase-separated liquid mixture is driven by the optical radiation pressure of the laser beam represented by the arrows. (C) Thinnest stable large aspect ratio liquid column obtained at $(T - T_C) = 4 K$ for a beam power $P = 410 mW$ and a waist $\omega_0 = 3.5 \mu m$. (D) Tuning of the liquid column diameter with further increase of the beam power to $P = 1134 mW$. The liquid column length is $334 \mu m$.